Journal of Physics: Conference Series

PAPER • OPEN ACCESS

Weak nuclear processes in the quest for elusive particles

To cite this article: O. Moreno 2020 *J. Phys.: Conf. Ser.* **1610** 012009

Journal of Physics: Conference Series **1610** (2020) 012009 doi:10.1088/1742-6596/1610/1/012009

Weak nuclear processes in the quest for elusive particles

O. Moreno

Departamento de Estructura de la Materia, Física Térmica y Electrónica and IPARCOS, Facultad de Ciencias Físicas, Universidad Complutense de Madrid, Ciudad Universitaria, 28040 Madrid, Spain, and Instituto de Estructura de la Materia, Consejo Superior de Investigaciones Científicas, Serrano 123, 28006 Madrid, Spain.

E-mail: osmoreno@ucm.es

Abstract.

Nuclear processes involving the weak interaction can be used to extract information on some elusive properties of particles. Remarkably useful to this goal is parity-violating elastic electron scattering off nuclei, which can be used to determine accurately the distribution of neutrons within the nucleus, including information on the neutron skin that can be related to the structure of neutron stars. It can also be used to determine the content of strange quark-antiquark virtual pairs in nucleons and can help in evaluating accurately Standard Model parameters or higher-order radiative corrections. To achieve these goals it is essential keeping under control the theoretical uncertainties that arise in modelling some confounding nuclear effects, such as isospin mixing or Coulomb distortion of electron wave functions.

The paradigm of an evasive particle in current physics is dark matter. Sterile neutrinos are hypothetical dark matter candidates that could be produced in nuclear beta decays leaving a signal in the energy spectrum of the emitted charged lepton. They can also be coherently scattered by nuclei through an indirect weak neutral interaction, whose cross section can be written in terms of elastic electron scattering observables. We study the probability of these production and detection mechanisms using experimental and cosmological constraints on the sterile neutrino properties.

The coherent scattering cross section off nuclei has also been analyzed for the Standard Model neutrinos, being a notably elusive process that has been recently measured for the first time and that can be used for Standard Model tests or for nuclear structure studies in ways analogous to parity-violating electron scattering.

1. Introduction

At the usual energies of lepton-nucleus scattering experiments the weak interaction is a few orders of magnitude weaker than the electromagnetic one. When only the weak interaction is involved in a given process, such as in neutrino scattering, cross sections are very small. If the electromagnetic interaction is also present, such as in electron scattering, the effect of the weak interaction is greatly, but not fully, overshadowed. In both cases, however, the analysis of the weak interaction effects can give very valuable information on some elusive properties of particles and nuclei that cannot be extracted with the desired level of precision from electromagnetic or strong processes, such as the neutron distribution in nuclei, the presence of strange content in nucleons, the coherent scattering of neutrinos by nuclei or the production and direct detection mechanisms for some dark matter candidates, among others.

Purely weak processes such as beta decay or charged-current neutrino-nucleus scattering are well known experimentally. Others, especially those based exclusively on the weak neutral current, were predicted long ago but have been measured recently for the first time. When the weak neutral interaction acts simultaneously with the electromagnetic interaction in a certain process, the small contribution of the former shows up in parity-violating observables, as we describe in what follows.

The weak current consists of two terms, both with the same relative weight: a vector term dependent on a four-vector of Dirac matrices, $\gamma^\mu = (\gamma^0, \gamma^1, \gamma^2, \gamma^3)$, and an axial term dependent on the same four-vector and an additional Dirac matrix factor, $\gamma^5\gamma^\mu$. Both behave differently under a parity transformation (inversion of coordinates), and when they mix, parity conservation is not fulfilled. In particular, when the electromagnetic and the weak interactions are both involved, the square of the probability amplitude mixes the purely-vector electromagnetic current with the axial term of the weak neutral current, giving rise to parity violation. This effect, however, can only be measured in specific experiments and with specific observables. One of such experiments is the elastic scattering of longitudinally polarized electrons, and the suitable observable is the parity-violating asymmetry (PVA), which is proportional to the difference between cross sections of electrons polarized parallel and antiparallel to their momentum, namely, with their spins and momenta aligned in the same or in opposite directions, respectively. These two situations are one the spatial inversion of the other and they yield different results if parity is not conserved. By denoting $d\sigma^+$ and $d\sigma^-$ the differential cross sections of electrons polarized parallel and antiparallel to their momentum, respectively, the PVA can be defined as:

$$\mathcal{A} = \frac{d\sigma^+ - d\sigma^-}{d\sigma^+ + d\sigma^-} \,, \tag{1}$$

which, under some approximations, can be written as [1]:

$$\mathcal{A} = \frac{1}{2\sqrt{2}\pi} \, \frac{G_F}{\alpha} \, \frac{W^{PV}}{W^{PC}} \, |Q^2| \tag{2}$$

It consists of three relevant factors: one containing the Standard Model (SM) electromagnetic and weak coupling constants (α and G_F, respectively); one containing the structure of the nuclear target through the ratio between its parity-violating response (W^{PV}) and its parity-conserving response (W^{PC}); and the four-momentum transfer squared ($|Q^2|$). This expression is valid in Born approximation, namely when one virtual gauge boson of each interaction (one photon and one Z^0) is exchanged, and in plane wave approximation, namely when the effect of the nuclear Coulomb field on the electron wave function is not taken into account and thus the latter is represented by a plane wave; both approximations together are denoted as PWBA (plane wave Born approximation). When the distortion of the electron wave function due to the nuclear Coulomb field is considered, the approximation is known as distorted wave Born approximation and denoted as DWBA.

The effective coupling of the weak interaction, given by the Fermi constant G_F, incorporates the propagator of the exchanged boson, which is inversely proportional to its mass for usual (low) energies. Due to the SM electroweak mixing, the weak effective coupling can be related to the electromagnetic coupling α as $G_F \approx (12.8/m_Z^2)\,\alpha$. Introducing the large mass of the Z^0 boson (91.2 GeV) one gets $G_F \sim 1.5 \cdot 10^{-9}\,\alpha$ (in MeV^{-2}). As a result, the PVA at momentum transfers of a few hundreds of MeV is of the order of 10^{-6}.

The parity-conserving response consists of electromagnetic (vector-vector) longitudinal (L) and transverse (T) terms, whereas the parity-violating response consists of mixed electromagnetic-weak terms of various types: longitudinal vector-vector (L), transverse vector-vector (T) and transverse axial-vector (T'). Each term contains a kinematic factor coming

from the electron current (generalized Rosenbluth factor), and a factor coming from the nuclear current, expressed in terms of nuclear form factors $F(q)$, where q is the momentum transferred from the electron to the nucleus. When the nuclear target has a spin 0 ground state, $J = 0$ (as is in all even Z - even N nuclei), only the longitudinal Coulomb-type monopole (C0) form factors play a role in the elastic scattering, both electromagnetic (EM) and weak neutral (WN):

$$F^{EM}_{(C0)}(q) = G^{EM}_p(q)\ Z\ F_p(q) + G^{EM}_n(q)\ N\ F_n(q)\ , \tag{3}$$

$$F^{WN}_{(C0)}(q) = G^{WN}_p(q)\ Z\ F_p(q) + G^{WN}_n(q)\ N\ F_n(q) \tag{4}$$

They contain nuclear form factors $F_{p,n}(q)$, which are the Fourier transform of the corresponding density distribution $\rho_{p,n}$ and fulfil $F_{p,n}(q \to 0) \to 1$, as well as electromagnetic and weak neutral nucleon form factors $G^{EM}_{p,n}(q)$ and $G^{WN}_{p,n}(q)$ (of electric type in both cases; the very small contribution of magnetic-type nucleon form factors can be seen in Ref. [2]). The EM and WN nucleon form factors are interrelated according to the SM electroweak mixing as:

$$G^{WN}_p(q) = \beta^p_V\ G^{EM}_p(q) + \beta^n_V\ G^{EM}_n(q)\ , \tag{5}$$

$$G^{WN}_n(q) = \beta^n_V\ G^{EM}_p(q) + \beta^p_V\ G^{EM}_n(q)\ , \tag{6}$$

where β^n_V and β^p_V are the weak neutral vector couplings of the Z^0 to neutrons and protons, respectively, whose SM values are $\beta^n_V = -1/2$ and $\beta^p_V = 1/2 - 2\sin^2\theta_W \approx 0.04$ (where θ_W is the weak mixing angle that defines the degree of mixing between the weak and the electromagnetic interactions).

In terms of the Coulomb monopole form factors in Eqs. 3 and 4, the ratio of responses in Eq. 2 for $J = 0$ nuclear targets can be written as:

$$\left.\frac{W^{PV}}{W^{PC}}\right|_{J=0} = a^e_A\ \frac{F^{WN}_{(C0)}(q)}{F^{EM}_{(C0)}(q)}\ , \tag{7}$$

where a^e_A is the axial coupling of the electron to the Z^0 boson, with a SM value of -1. By neglecting the small neutron electric form factor G^{EM}_n, Eq. 7 can be written as:

$$\left.\frac{W^{PV}}{W^{PC}}\right|_{J=0} \approx a^e_A\ \frac{\left(\beta^n_V\ F_n(q)\ N + \beta^p_V\ F_p(q)\ Z\right)}{F_p(q)\ Z} = a^e_A\ \beta^n_V\ \frac{N}{Z}\ \left(\frac{F_n(q)}{F_p(q)} + \frac{\beta^p_V}{\beta^n_V}\frac{Z}{N}\right) \tag{8}$$

By further neglecting the small term $\beta^p_V Z/\beta^n_V N$ in the previous expression, whose absolute value lies between ∼0.05 and ∼0.08, and introducing the SM values of the electron and nucleon couplings, the full PVA results [3]:

$$\mathcal{A}|_{J=0} \approx \frac{1}{4\sqrt{2}\pi}\ \frac{G_F}{\alpha}\ \frac{N}{Z}\ \frac{F_n(q)}{F_p(q)}\ |Q^2| \tag{9}$$

A nucleus with an isospin 0 ground state, $T = 0$, contains the same number of protons and neutrons, $N = Z$, and they behave exactly in the same way within the nucleus, resulting in $F_p(q) = F_n(q)$. For such a nuclear target Eq. 8 becomes [4]:

$$\left.\frac{W^{PV}}{W^{PC}}\right|_{J,T=0} = a^e_A\ (\beta^n_V + \beta^p_V) = 2\ \sin^2\theta_W \tag{10}$$

The corresponding PVA, which is valid in PWBA for $J, T = 0$ targets, is:

$$\mathcal{A}|_{J,T=0} = \frac{1}{\sqrt{2}\pi}\ \frac{G_F}{\alpha}\ \sin^2\theta_W\ |Q^2| \tag{11}$$

2. Neutrons in nuclei

The well known electroweak theory behind parity-violating electron scattering allows for the study of the neutron distribution in nuclei with better precision than using hadronic probes. In addition, weak neutral processes are more sensitive to the neutron distribution because the vector coupling of the Z^0 to neutrons is more than twelve times larger than to protons.

The root mean square radius of neutrons in a nucleus, $\hat{r}_n$, can be extracted from PVA and proton form factor measurements using Eq. 9. The proton form factor can be determined accurately from usual (parity-conserving) electron scattering experiments, whereas the PVA can be measured in polarized electron scattering, as described in the previous section. In a realistic procedure one should use a numerical relationship between the measured PVA and F_p that takes into account the Coulomb distortion of the electron wave function (through a DWBA calculation) and the nucleon form factors, effects that were not considered in Eq. 9. Measurements of the PVA at several momentum transfers could help determine more accurately the neutron root mean square radius (through $\hat{r}_n \approx -6\, dF/d(q^2)$ at small q) or the neutron density distribution through the inverse Fourier transform of the neutron form factor. However, PVA measurements of the order of $\sim 10^{-6}$ need large statistics, which is very difficult to reach with polarized electron beams; therefore, experiments nowadays focus on just one value of the momentum transfer and direct theoretical model comparisons are then used to extract $\hat{r}_n$.

As an illustration of the steps involved in the determination of the neutron distributions in nuclei we show in Figs. 1-3 results for three stable barium isotopes: ^{130}Ba, ^{134}Ba, and ^{138}Ba [5]. This element is interesting for parity violation experiments because it has seven stable or very long-lived isotopes, which allow us to study the evolution of neutron distribution features in a long isotopic chain, from 74 to 82 neutrons. In addition, barium atoms are relevant for atomic parity violation studies, namely the parity mixing in the wave functions of bound electrons, that shows up as nominally-forbidden atomic transitions [5]. The results for the barium isotopes shown in Figs. 1-3 have been obtained from an axially deformed Hartree-Fock mean field calculation using SLy4 Skyrme nucleon-nucleon interactions and pairing within BCS approximation. We obtain deformed (prolate) ground-state shapes in ^{130}Ba and ^{134}Ba and spherical shape in ^{138}Ba (which contains a magic number of neutrons, 82).

In Fig. 1 we show the neutron and proton spherical density distributions obtained from the calculation mentioned above. As the number of neutrons increases in the isotopic chain, they tend to accumulate in the outer region of the nucleus, thus increasing the root mean square radius of neutrons, $\hat{r}_n$, whereas the one for protons, $\hat{r}_p$, hardly changes. This neutron-rich outer region is known as neutron skin, whose thickness is given by $\hat{R} = \hat{r}_n - \hat{r}_p$. In the barium isotopes under study $\hat{R}$ increases from 0.075 fm in ^{130}Ba to 0.102 fm in ^{134}Ba and to 0.147 fm in ^{138}Ba; these numbers represent a $\sim 40\%$ increase for every $\sim 5\%$ increase in the number of neutrons.

The neutron skin arises from a competition between different contributions to the nuclear energy. On the one hand, the asymmetry energy contribution, that favors an equal distribution of protons and neutrons, is more important where the nucleon density is larger, namely in the inner region; as a consequence, the neutron excess in medium and heavy nuclei tends to be pushed out of that symmetric core towards the less dense outer region. The presence of a Coulomb barrier also plays a role in confining the protons within that core. On the other hand, there is a surface energy contribution that tends to compress the neutron excess back to the symmetric core to reduce the surface tension of the nucleus.

In Fig. 2 we show the form factors corresponding to the proton and neutron density distributions of Fig. 1, as a function of the momentum transfer in inverse fermi ($1\ \mathrm{fm}^{-1} = 197.3$ MeV). Finally, in Fig. 3 we give for the same isotopes the PVA for polarized elastic electron scattering again as a function of the momentum transfer in inverse fermi; it has been obtained in PWBA from the form factors shown in Fig. 2, using Eq. 9.

Following this procedure in the inverse direction, the PREX and CREX series of experiments

at Jefferson Lab [6] are aimed at extracting information on the neutron distribution, particularly the neutron skin thickness, of ^{208}Pb and ^{48}Ca, respectively, from the measured PVA in polarized electron elastic scattering.

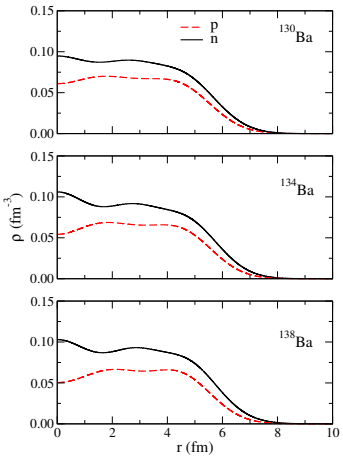

Figure 1. Neutron density (solid line) and proton density (dashed line) of the stable barium isotopes ^{130}Ba, ^{134}Ba, ^{138}Ba as a function of the radial coordinate.

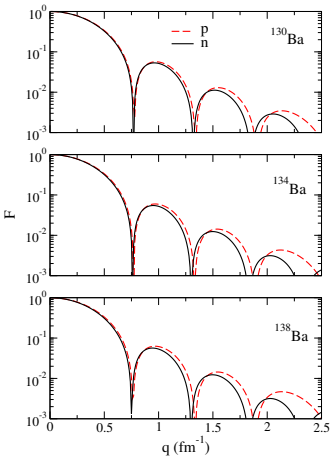

Figure 2. For the same barium isotopes of Fig. 1, neutron form factor (solid line) and proton form factor (dashed line) as a function of the momentum transfer.

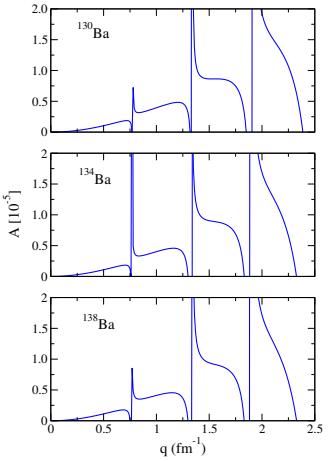

Figure 3. For the same barium isotopes of Fig. 1, PVA for polarized electron elastic scattering as a function of the momentum transfer.

2.1. Neutron matter equation of state and neutron stars

A neutron star is an astrophysical object with a radius of around 10 km and a mass of the order of the solar mass, held together by gravity. The outer region is a solid crust, 1 to 2 km thick, made of neutron-rich nuclei, with more topologically-complex structures arising as the density increases with depth. The outer core, located below the crust, is made of a homogeneous fluid of neutrons with a small proportion of protons and charged leptons (electrons, muons), with densities close to the nuclear saturation density [7]. Neutron stars are supported against gravitational collapse by the same pressure that gives rise to neutron skins in nuclei, and therefore experimental information on the latter can be used to predict some features of the former.

Pressure is a magnitude of the nuclear equation of state that reflects how the energy per nucleon, ε, changes as a function of the density of nucleons, ρ: $P \propto d\varepsilon/d\rho$; the larger the pressure, the faster the energy increase with density. The energy per nucleon can be written as $\varepsilon(\rho) \approx \varepsilon_S(\rho) + \xi^2\, \varepsilon_A(\rho)$, where ε_S is the energy for symmetric nuclear matter ($\rho_n = \rho_p$), $\varepsilon_A(\rho)$ is the asymmetry energy and $\xi = (\rho_n - \rho_p)/(\rho_n + \rho_p)$ is the proton-neutron asymmetry.

In neutron stars, the most relevant role is played by the pressure of pure neutron matter ($\xi = 1$) at saturation density ρ_0, which is proportional to the variation of the asymmetry energy with the density of nucleons at ρ_0: $P_N(\rho_0) \propto (d\varepsilon_A/d\rho)|_{\rho_0}$; this result makes use of the fact that ρ_0 is the equilibrium density of nuclei (which are nearly symmetric systems) and thus $(d\varepsilon_S/d\rho)|_{\rho_0} = 0$ [7]. As explained above, the formation of a neutron skin in nuclei originates also from the differences in asymmetry energy between regions with different density, leading to $\hat{R} \propto (d\varepsilon_A/d\rho)|_{\rho_0}$. According to this, one can predict under some reasonable assumptions that the thicker the neutron skin $\hat{R}$, the larger the neutron matter pressure at saturation density

$P_N(\rho_0)$ and therefore the larger the radius of neutron stars. Moreover, the thicker the neutron skin, the thinner the crust of neutron stars, because a phase change from solid to fluid (from crust to core) becomes favorable at a lower density, *i.e.* closer to the star surface [8].

3. Strange quark content in nucleons

If there exists a nonzero vector contribution in the nucleon due to strange sea quarks, $\bar{s}\gamma^\mu s$, then the weak neutral nucleon form factors of Eqs. 5-6 have an extra term explicitly dependent on a strangeness electric form factor, in addition to the electric proton and neutron form factors:

$$G_p^{WN}(q) = \beta_V^p\, G_p^{EM}(q) + \beta_V^n\, G_n^{EM}(q) + \frac{1}{2}\,\beta_V^{(s)}\, G_{(s)}^{EM}(q)\,, \tag{12}$$

$$G_n^{WN}(q) = \beta_V^n\, G_p^{EM}(q) + \beta_V^p\, G_n^{EM}(q) + \frac{1}{2}\,\beta_V^{(s)}\, G_{(s)}^{EM}(q)\,, \tag{13}$$

where, in the SM, $\beta_V^{(s)} = -1$.

This additional contribution due to strangeness has an effect on the PVA, which can be analyzed more easily using an isospin 0 nuclear target. To this end, it is convenient to define the PVA deviation due to the strangeness content of the nucleon, Γ^s, as the relative difference between the PVA with strangeness, $\mathcal{A}|_{J,T=0}^{(s)}$, and without strangeness (given in Eq. 11):

$$\Gamma^s = \frac{\mathcal{A}|_{J,T=0}^{(s)} - \mathcal{A}|_{J,T=0}}{\mathcal{A}|_{J,T=0}} = \frac{\beta_V^{(s)}}{(\beta_V^p + \beta_V^n)}\,\frac{G_{(s)}^{EM}(q)}{\left[G_p^{EM}(q) + G_n^{EM}(q)\right]} \tag{14}$$

Reasonable momentum transfer dependences, such as dipole or monopole, can be assumed for the nucleon strangeness form factor, but at small momentum transfer one has $G_{(s)}^{EM}(q) \propto \rho_s |Q^2|$, where the parameter ρ_s is the electric strangeness content of the nucleon. It can be extracted from parity-violating electron scattering measurements on simple targets such as a the proton, deuterium or helium 4. Current experimental data give a range of ρ_s at the 2σ level ($\sim 95\%$) roughly between $+1.6$ and -0.4, centered at $+0.6$, and compatible with zero [9]. This is the range used in Fig. 4, which shows the asymmetry deviation due to the nucleon strangeness content, Γ^s (Eq. 14), as a function of the momentum transfer [10].

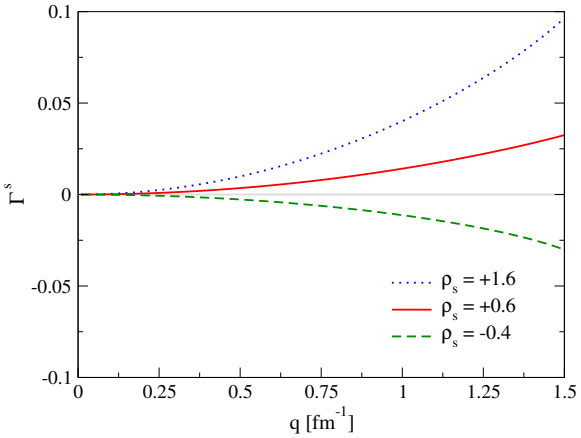

Figure 4. PVA deviation due to nucleon strangeness, for different values of the strangeness content parameter ρ_s, for an isospin 0 nuclear target, as a function of the momentum transfer.

3.1. Standard Model tests

The simplicity of Eq. 11 can be used to extract accurate values of SM parameters, such as the weak mixing angle θ_W, or the size and momentum-dependence of higher-order electroweak radiative corrections. The procedure consists of measuring the PVA in elastic electron scattering by $N = Z$ nuclei and compare it with the reference value given by Eq. 11 through a deviation analogous to Eq. 14, in order to find discrepancies between the measurements and the current theoretical knowledge. Of course, this method requires a good theoretical control of the deviations arising from nuclear or nucleon structure effects that are not considered in Eq. 11. Among the latter one finds isospin mixing in the nuclear ground state, nonzero strangeness content in the nucleon, distortion of the incoming and outgoing electron wave functions due to the nuclear Coulomb field, meson exchange currents between nucleons, or inelastic contaminations if the energy resolution of the detector is poor. It should be recalled that Eq. 11 was obtained for a pure (non-mixed) isospin 0 nuclear target without strangeness content nor meson exchange currents, in PWBA (without Coulomb distortion) and for purely elastic electron scattering.

In order to estimate the current theoretical knowledge on nuclear and nucleon structure effects on PVA that could spoil accurate SM tests, we have computed their size and corresponding theoretical uncertainties for a ^{12}C target (nominally $T = 0$) with polarized electrons at 150 MeV incident energy and $q \sim 100$ MeV momentum transfer [10]. The distortion of the electron wave function due to the nuclear Coulomb field introduces a 3% change in the reference PVA of Eq. 11, with a very small relative uncertainty (of the order of 0.01%), since the theory that accounts for the distortion (DWBA) is very accurate. The isospin mixing of electromagnetic origin in the ground state of ^{12}C introduces a 0.4% change in the reference PVA, with a small theoretical uncertainty of the order of 0.05%. The possible strangeness content of the nucleon modifies the reference PVA up to a 1%, as seen in Fig. 4: $|\Gamma^s(q \approx 0.5\,\mathrm{fm}^{-1})| \lesssim 0.01$. As we explained above, this spread in Γ^s comes from the experimental uncertainty in the strangeness content parameter ρ_s, so the uncertainty in modelling the effect of strangeness is actually that full 1%. Finally, the possible presence of meson exchange currents between nucleons and the possible contribution of inelastic transitions account both for up to a 0.1% change in the reference PVA, with a theoretical uncertainty of the same level.

Several experimental facilities have been proposed recently to measure accurately the PVA at small momentum transfer, using low-energy, high-luminosity polarized electron beams, such as MESA in Mainz, FEL at Jefferson Laboratory or Cβ at Cornell University [11]. Their primary goal is to perform SM tests, for which they should measure the PVA with a precision of a few tenths of percent. To this end, the theoretical uncertainty in the description of the confounding nuclear and nucleon structure effects should reach the same level of precision.

As presented above, the current uncertainty in the contribution of strange sea quarks to the PVA is the only effect that clearly exceeds the desired limit of precision. In order to pin down the nucleon strangeness content one could measure the PVA using a nuclear target with small isospin mixing (to avoid confounding), such as ^{4}He, at momentum transfers where the effect on the PVA is large but far from the diffraction minima of the nuclear form factors. At that point, $q \sim 300$ MeV, a measurement of the PVA with 2% precision would reduce the strangeness uncertainty to that level, and then it would scale down (as q^2) to the required few tenths of percent for small momentum transfers.

4. Dark matter production and direct detection

In the SM, the neutrino flavor eigenstate emitted in beta minus decay together with an electron, $|\nu_e\rangle$, is a linear combination of three neutrino mass eigenstates, that we will consider from now on as just one light mass eigenstate, $|\nu_l\rangle$, with mass $m_l \approx 0$ (but $m_l \neq 0$). An additional, hypothetical heavy mass eigenstate, $|\nu_h\rangle$, can be assumed to exist so that the electron neutrino flavor can be written approximately as the linear combination $|\nu_e\rangle = \cos\theta_{lh}\,|\nu_l\rangle + \sin\theta_{lh}\,|\nu_h\rangle$,

where the parameter θ_{lh} is the light/heavy mixing angle. The concept of sterile neutrino refers to the new, hypothetical flavor eigenstate that results from the linear combination of mass eigenstates orthogonal to the previous one: $|\nu_s\rangle = \sin\theta_{lh}\,|\nu_l\rangle - \cos\theta_{lh}\,|\nu_h\rangle$. This additional neutrino flavor is not associated with any charged lepton, in contrast to the three active SM neutrinos. In other words, $|\nu_s\rangle$ is a SU(2) weak-isospin singlet, resulting in no direct weak interaction, whether charged or neutral. The lack of all SM couplings in $|\nu_s\rangle$ would prevent its direct detection, showing only gravitational effects, which are the features commonly attributed to dark matter.

The small content of $|\nu_h\rangle$ in the electron neutrino could leave a signature, for instance, in the energy spectrum of the electron emitted in beta decay. The most promising nuclei to measure this hypothetical effect are the same that have been used to determine the mass of active neutrinos, due to their small Q-value that helps improve the statistics: ^{3}H ($Q_\beta = 18.6$ keV) in KATRIN experiment and ^{187}Re ($Q_\beta = 2.47$ keV) in MARE experiment.

As an illustration of the effect of a heavy neutrino emission in nuclear beta decay we show in Fig. 5 for the decay of ^{187}Re the relative difference between the electron spectrum when a heavy neutrino eigenstate contributes to $|\nu_e\rangle$ ($\theta_{lh} \neq 0$) and when it does not ($\theta_{lh} = 0$), given by [12]:

$$\eta = \left(N_{[\theta_{lh}\neq 0]} - N_{[\theta_{lh}=0]}\right)/N_{[\theta_{lh}=0]} \tag{15}$$

We have used in Fig. 5 a heavy neutrino mass $m_h = 1$ keV, which can be produced whenever the electron emitted by ^{187}Re carries a kinetic energy lower than $Q_\beta - m_h = 1.47$ keV. At that point, corresponding to an electron momentum $p_e = 38.79$ keV, a drastic change in the ratio η takes place, proportional to $\sin^2\theta_{lh}$. We have chosen a mixing angle $\theta_{lh} = 0.005°$ ($\sin^2\theta_{lh} \sim 10^{-8}$), which is un upper limit derived from several experimental and observational data [13] for a neutrino mass $m_h = 1$ keV.

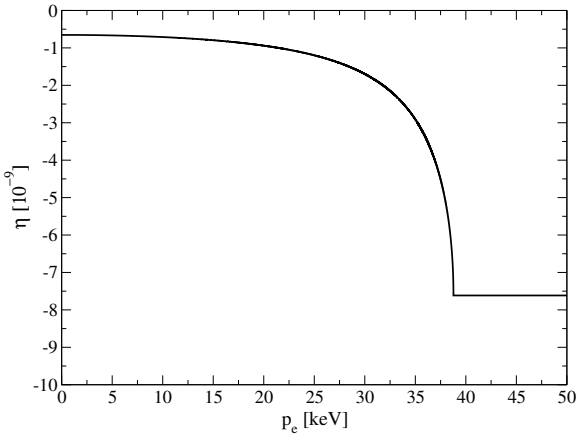

Figure 5. For the spectrum of the electron emitted in the beta decay of ^{187}Re, relative difference η (Eq. 15) between presence (with $\theta_{lh} = 0.005°$) and absence ($\theta_{lh} = 0$) of a heavy neutrino component of mass $m_h = 1$ keV in the electron neutrino.

As mentioned above, sterile neutrinos have the required properties to be part of the dark matter content of the universe. Some cosmological and astrophysical observations support the warm dark matter hypothesis, namely dark matter particles with masses in the keV range (see [12] and references therein), which is the reason why we have chosen a mass $m_h = 1$ keV. Other observations introduce some tension concerning the production of sterile neutrinos in the early universe, but several theoretical mechanisms have been proposed to overcome the disagreement, among them the interaction with non-SM fields resulting in a dynamical weak mixing angle [14].

Dark matter particles have never been directly detected, which implies that their couplings with ordinary matter should be much smaller than the SM ones. The direct detection of sterile neutrinos, that are suitable dark matter candidates, would be of utmost interest. One possible mechanism would be their coherent scattering with nuclei, to which all the nucleons in the target contribute and where the nuclear target remains in its ground state (elastic process); the latter implies that the only effect that can be detected is the nuclear recoil, which is usually very small. It occurs in spin 0, isospin 0 targets ($J, T = 0$) at momentum transfers with associated de Broglie wavelengths of the order of the nuclear size, $q \approx 160\, A^{-1/3}$ MeV. For targets $J, T \neq 0$, the coherent is not the only contribution to the elastic scattering, but is usually dominant except for very light nuclei.

The differential cross section of the coherent scattering of a heavy mass neutrino can be computed as an extension of the SM calculation for active neutrinos. Interestingly, this cross section can be related to well known electron elastic scattering observables: the PVA in polarized electron elastic scattering and the differential cross section of unpolarized electron elastic scattering by $J = 0$ nuclei, as follows [15]:

$$\left(\frac{d\sigma}{d\Omega}\right)_{\nu_h} = \sin^2\theta_{lh}\,\frac{1}{2}\,(\mathcal{C}_V + \mathcal{C}_A)\;\mathcal{A}^2\;\left(\frac{d\sigma}{d\Omega}\right)_e\,, \tag{16}$$

where $\mathcal{C}_V$ and $\mathcal{C}_A$ are vector and axial kinematic factors that depend on the incident energy and scattering angle of the electron in the PVA and in the cross section, as well as on the heavy neutrino mass and on the nuclear target mass.

In Fig. 6 we show the elastic scattering integrated cross section of the heavy neutrino with a ^{12}C target, as a function of the incident velocity ($\beta = v/c$) of the neutrino. The same heavy neutrino properties as in the production observable of Fig. 5 have been used here, namely mass $m_h = 1$ keV and mixing angle $\theta_{lh} = 0.005°$. This calculation comes from the integration to all scattering angles of the differential cross section in Eq. 16, and has been separated into a vector term (proportional to $\mathcal{C}_V$) and an axial term (proportional to $\mathcal{C}_A$).

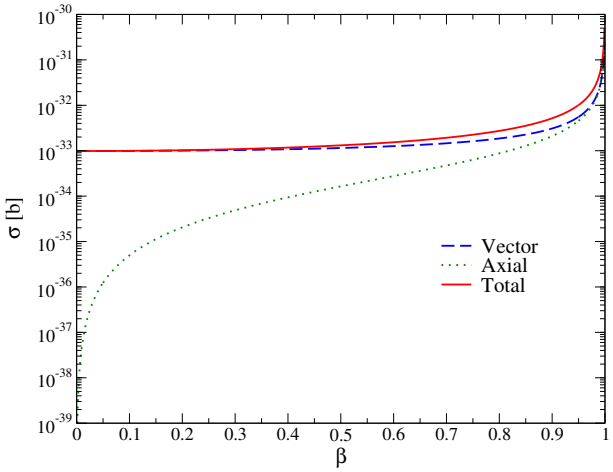

Figure 6. Vector (dashed line) and axial (dotted line) contributions to the integrated cross section (solid line) of elastic scattering of the heavy neutrino with a ^{12}C target, as a function of the velocity ($\beta = v/c$) of the neutrino. The heavy neutrino mass is $m_h = 1$ keV and the mixing angle is $\theta_{lh} = 0.005°$.

The differential cross section in Eq. 16 can be generalized to other dark matter particles that interact through a combination of vector and axial currents, as in the SM weak interaction but

with different couplings to the exchanged boson, that can be a Z^0 or a non-SM boson [15]:

$$\left(\frac{d\sigma}{d\Omega}\right)_{DM(V+A)} = \frac{\kappa^2\,(\gamma_V^p+\gamma_V^n)^2}{G_F^2\,(\beta_V^p+\beta_V^n)^2}\,\frac{1}{2}\left(b_V^2\,\mathcal{C}_V + b_A^2\,\mathcal{C}_A\right)\,\mathcal{A}^2\,\left(\frac{d\sigma}{d\Omega}\right)_e\,, \tag{17}$$

where $\gamma_V^{p,n}$ are the hadronic couplings and $b_{V,A}$ are the dark matter couplings to the new boson that mediates the dark matter interaction, and κ is the overall coupling.

4.1. Standard Model neutrinos

The expressions in Eqs. 16 or 17 can be particularized to the coherent scattering of active neutrinos, that have the SM couplings: $\gamma_V^{p,n} = \beta_V^{p,n}$, $b_{V,A} = a_{V,A}^{\nu} = 1$, $\kappa = G_F$; due to their small masses, the extreme relativistic limit applies, for which $\mathcal{C}_{V,A} \to 1$. Thus, the active neutrino elastic differential cross section becomes very simple when expressed in terms of the electron scattering magnitudes for $J = 0$ targets [16]:

$$\left(\frac{d\sigma}{d\Omega}\right)_{\nu} = \mathcal{A}^2\,\left(\frac{d\sigma}{d\Omega}\right)_e \tag{18}$$

Coherent neutrino scattering was predicted more than 40 years ago, but the first detections have been registered only very recently in the COHERENT experiment [17]. Although the cross section is larger than for other neutrino-nucleus interactions, being proportional to the mass number (especially the neutron number) squared due to coherence, the nuclear recoil energy is very small and therefore hard to detect. The situation is obviously worse for the direct detection of the heavy neutrino or other similar dark matter candidates, since for them the cross sections themselves are very small. Experimental data on neutrino coherent scattering can be used to evaluate SM electroweak constants at low momentum transfers, such as the weak mixing angle [18], as well as the size and momentum-dependence of higher-order corrections, to test the universality of the weak neutral interaction for different leptons, to obtain information on the axial structure of the nuclear target or to understand core collapses, supernova explosions or cooling mechanisms in some types of stars.

[1] Donnelly T W, Dubach J and Sick I 1989 *Nucl. Phys.* A **503** 589
[2] Moreno O, Sarriguren P, Moya de Guerra E, Udias J M, Donnelly T W and Sick I 2009 *Nucl. Phys.* A **828** 306
[3] Moreno O, Sarriguren P, Moya de Guerra E, Udias J M, Donnelly T W and Sick I 2011 *J. Phys.: Conf. Ser.* **312** 092044
[4] Feinberg G 1975 *Phys. Rev.* D **12** 3575; Walecka J D 1977 *Nucl. Phys.* A **285** 349
[5] Moreno O, Navarro De Martino E, Moya de Guerra E and Sarriguren P 2013 *Rom. Journ. Phys.* **58** 1270
[6] Abrahamyan S *et al.* (PREX Collaboration) 2012 *Phys. Rev. Lett.* **108** 112502; hallaweb.jlab.org/parity/prex
[7] Piekarewicz J 2016 *Relativistic Density Functional Theory for Finite Nuclei and Neutron Stars* (Relativistic Density Functional Theory for Nuclear Structure) ed J Meng (Singapore: World Scientific Publishing Company) chapter 14 pp 625–658
[8] Horowitz C J and Piekarewicz J 2001 *Phys. Rev. Lett.* **86** 5647
[9] Gonzalez-Jimenez R, Caballero J A and Donnelly T W 2013 *Phys. Rep.* **524** 1
[10] Moreno O and Donnelly T W 2014 *Phys. Rev.* C **89** 015501
[11] Aulenbacher K 2011 *Hyperfine Interact.* **200** 3; Neil G R *et al.* 2000 *Phys. Rev. Lett.* **84** 662; Bazarov I *et al.* 2015 physics.acc-ph/1504.00588
[12] de Vega H J, Moreno O, Moya de Guerra E, Ramon Medrano M and Sanchez N G 2013 *Nucl. Phys.* B **866** 177
[13] Kusenko A 2009 *Phys. Rep.* **481** 128
[14] Berlin A and Hooper D 2017 *Phys. Rev.* D **95** 075017
[15] Moreno O and Donnelly T W 2016 *Preprint* hep-ph/1603.05932v1
[16] Moreno O and Donnelly T W 2015 *Phys. Rev.* C **92** 055504
[17] Akimov D *et al.* (COHERENT Collaboration) 2017 *Science* **357** 1123
[18] Cañas B C, Garcés E A, Miranda O G and Parada A 2018 *Phys. Lett.* B **784** 159